



ELSEVIER

Geomorphology 45 (2002) 105–125

GEOMORPHOLOGY

www.elsevier.com/locate/geomorph

Quantifying sediment transport on desert piedmonts using ^{10}Be and ^{26}Al

Kyle K. Nichols^{a,*}, Paul R. Bierman^a, Roger LeB. Hooke^b,
Erik M. Clapp^a, Marc Caffee^c

^aSchool of Natural Resources and Department of Geology, University of Vermont, Burlington, VT, 05405, USA

^bDepartment of Geological Sciences and Institute for Quaternary Studies, University of Maine, Orono, ME, 04496, USA

^cCenter for Accelerator Mass Spectrometry, Lawrence Livermore National Laboratory, Livermore, CA, 94550, USA

Received 10 September 1999; received in revised form 17 July 2001; accepted 5 October 2001

Abstract

In situ produced ^{10}Be and ^{26}Al , measured in 40 sediment samples collected from the Iron and Granite Mountain piedmonts, eastern Mojave Desert, provide a unique view of piedmont modification processes and process rates over the 10^3 to 10^5 year time scale. Cosmogenic nuclide-based models suggest that the Iron and Granite Mountains generate 0.11–0.13 and 0.082–0.097 m^3 of sediment per year per meter of range front, respectively. The sediment moves down the piedmont in an active transport layer (ATL), which is 20 to 30 cm thick (based on visual observations, measurements of depth to a buried B-horizon, cosmogenic nuclide data, and maximum ephemeral channel depths). Sediment in this layer is well-mixed vertically and horizontally on the 10^2 year time scale, indicating that the small ephemeral channels, which dominate the piedmont surface migrate quickly. Interpretive models of increasing nuclide activities at depth in two pits suggest steady sediment deposition on the piedmont (at rates between 17–21 and 38–45 m Ma^{-1}) until the late Pleistocene epoch, when a discontinuity to markedly lower nuclide activities in the isotopically well-mixed active transport layer suggests that deposition stopped, a significant change in piedmont behavior. Nuclide activities in 10 amalgamated surface samples, each collected along a different 4-km-long transect, increase steadily away from the mountain front. Thus, we infer that sediment is uniformly dosed by cosmic rays as it is transported down the Iron and Granite Mountain piedmonts. Interpretive models suggest that long-term average sediment speeds down the Iron and Granite Mountain piedmonts are a few decimeters to a meter per year. © 2002 Published by Elsevier Science B.V.

Keywords: Arid region sediment transport; Climate change; Cosmogenic nuclide; Desert geomorphology; Pediment; Piedmont

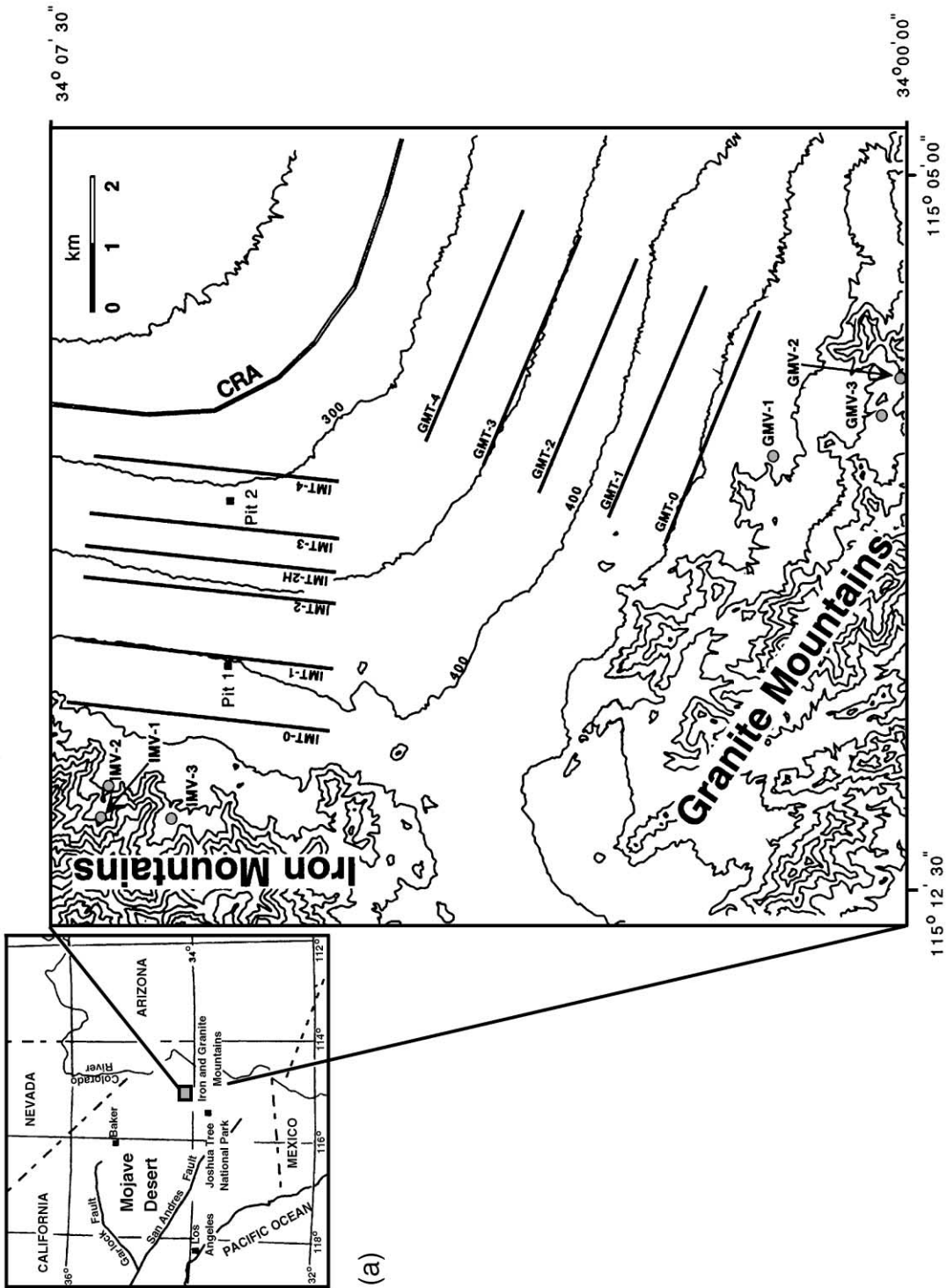
1. Introduction

Little is known about the rate and style of long-term sediment transport across desert piedmont surfaces (Denny, 1967; Hooke, 1968). Runoff is episodic in arid regions; thus, long-term observations, accom-

plished so far in only a few places worldwide, are necessary to determine process rates. Rates determined over these human time scales may or may not be representative of rates on geologic time scales (Greenbaum et al., 1999; Lekach and Schick, 1999; Yair, 1999). Furthermore, the difficulty in determining accurate sediment generation rates in source basins has precluded quantitative estimates of sediment flux and sediment transport rates across piedmont surfaces.

* Corresponding author.

E-mail address: kknichol@zoo.uvm.edu (K.K. Nichols).



(b)

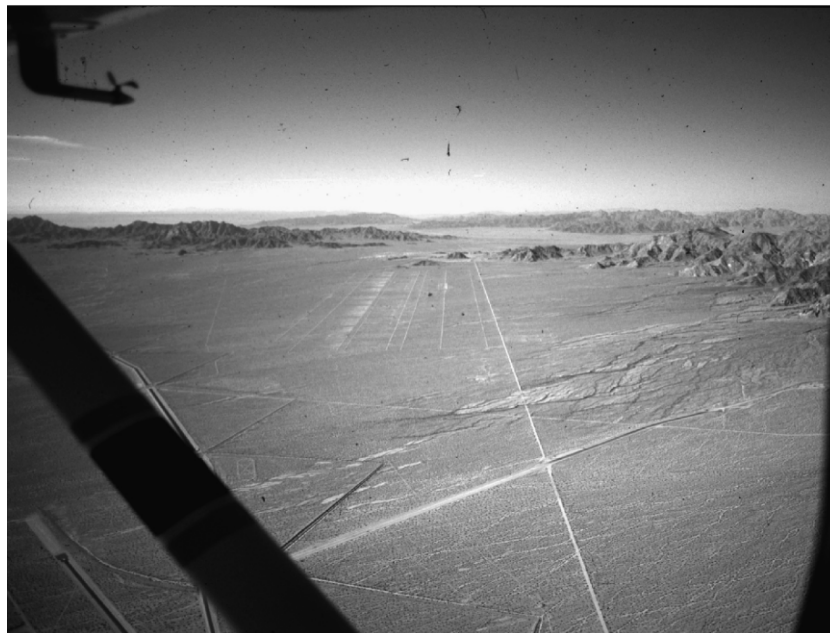


Fig. 1. (a) Location of the Iron and Granite Mountains in the Mojave Desert, CA, and detailed contour map of the Iron and Granite Mountain piedmonts. On the contour map, straight black lines represent transect locations on the piedmont surfaces. IMT=Iron Mountain transect samples, GMT=Granite Mountain transect samples, IMT-2H=Iron Mountain transect where additional shallow pits were dug, but no sediment samples collected. Black squares represent soil pit locations. Gray circles represent valley sample locations. IMV=Iron Mountain valley samples and GMV=Granite Mountain valley samples. CRA=Colorado River Aqueduct. Contour interval is 50 m. Map based on the Granite Pass and East of Granite Pass U.S.G.S. 1:24,000 Quadrangles, 1985. (b) Oblique aerial photograph of the Iron and Granite Mountains and respective piedmonts looking to the southwest. Granite Mountains are on the left (south) and the Iron Mountains are on the right (west). Steep, narrow source basins for each piedmont penetrate mountains normal to range front. View is ~ 10 km wide.

Traditional geomorphic techniques of mapping, monitoring, and observing soil development have elucidated surface histories and piedmont ages. These are useful for inferring changes in piedmont process (Birkeland, 1984; Wells et al. 1987; McFadden et al., 1989; Bull, 1991), changes that are routinely attributed to climatic fluctuations (Oberlander, 1974; Mayer and Bull, 1981; Dohrenwend, 1987; Bull, 1991). For example, Bull and Schick (1979) and Bull (1991) suggested that soil was stripped off desert hillslopes and transported down gradient as a result of the change from a wetter to a drier climate at the Pleistocene/Holocene transition. Similarly, Wells et al. (1987) associated increased drainage basin sediment yield with early Holocene deposition on piedmonts. They suggested that, once the reservoir of sediment stored in mountain

basins was depleted, transport capacity of channels increased and at least some piedmonts were dissected.

Previous studies of desert piedmonts have been unable to address the long-term rate and distribution of germane surface processes such as sediment transport and deposition. By using a new tool, in situ produced cosmogenic ^{10}Be and ^{26}Al , a novel sampling strategy, and interpretive models, we quantify long-term average sediment transport rates across large, planar, piedmont surfaces that extend more than 10 km from the Iron and Granite Mountains in the Mojave Desert, California (Fig. 1). Application of these techniques elsewhere could lead to a better understanding of arid-region sediment transport and surface processes on desert piedmonts including the effects of climate change.

2. Research area

In the Mojave Desert, the Iron and Granite Mountains rise steeply from adjacent, low-gradient ($\sim 2^\circ$) piedmonts (Fig. 1). The piedmont surfaces consist primarily of grus, 0.5 to 1 mm in diameter. There is minimal carbonate development in the soils (Fig. 2). Small ephemeral channels, averaging 10 cm in depth (Nichols and Bierman, 2002), migrate across the planar piedmonts and account for the majority of sediment transport (Bull, 1977). Almost all surface clasts are unvarnished; desert pavements are not well developed and there is no significant channel incision. These and other field observations suggest that the ephemeral channel network has relatively recently reworked most ($>98\%$) of the piedmont surface. The remainder, directly abutting the range front, is relict alluvium exhibiting some pavement development and incision by channels 0.5 to 5 m deep. There is no evidence for range-bounding faults, suggesting that the basin and adjacent ranges are not currently tectonically active.

The southern Mojave Desert and the Iron and Granite Mountain piedmonts are extremely dry and warm. Average annual precipitation is 79 mm and the mean temperatures for January and July are 12 and 35 °C, respectively (NOAA, 1982). Packrat midden data indicate a change in the climate from wetter to drier conditions between 10,000 and 8000 years ago (Spaulding et al., 1983; Spaulding and Graumlich, 1986).

3. Cosmogenic nuclides

Cosmic rays bombard Earth's surface and produce a variety of nuclides in situ including ^{10}Be and ^{26}Al . Cosmogenic nuclide production rates are greatest at the surface and decrease exponentially with depth (Lal, 1988). For example, production rates at a depth of 1 m in sediment ($\rho = 1.55 \text{ g cm}^{-3}$) are 37% of surface production. Production rates for ^{10}Be and ^{26}Al , and the adjustments for altitude and latitude, have been estimated, but remain uncertain at the 10% to 20% level (Nishiizumi et al., 1989; Lal, 1991; Clark et al., 1995; Bierman et al., 1996; Dunai, 2000; Desilets and Zereda, 2000). We can measure ^{10}Be and ^{26}Al activities (to $\pm 4\%$ precision or better) using accelerator mass spectrometry. We use these nuclides as cosmic-

ray dosimeters to record near-surface residence time. Using quantitative and qualitative geomorphic models, we interpret measured ^{10}Be and ^{26}Al activities in terms of integrated cosmic-ray dosing. From this information, we estimate sediment transport rates expressed as average grain speeds down piedmont.

4. Methods

4.1. Sediment collection for ^{10}Be and ^{26}Al analysis

To understand and quantify the three-dimensional behavior of the Iron and Granite Mountains and their piedmonts over time, we collected three types of samples: source valley alluvial sediment, piedmont surface sediment, and sediment exposed in soil pits. Measurement of ^{10}Be and ^{26}Al in sediment samples collected from valleys at the Iron and Granite Mountain range fronts allows quantification of long-term average source-basin lowering rates and the flux of sediment entering the piedmont (e.g., Brown et al., 1995; Bierman and Steig, 1996; Granger et al., 1996). Integrated piedmont transect samples located at successive 1-km intervals from the range front reflect changes in average ^{10}Be and ^{26}Al activity as sediment moves away from the source basins and allow us to determine average sediment speed down piedmont. Profiles of piedmont sediment exposed in soil pits allow us to quantify the depth to which sediment is currently well mixed and provide insight into whether the piedmont is, or has been, a surface of deposition, erosion, or transport.

4.1.1. Source valley alluvial sediment samples

We determined long-term basin erosion and sediment generation rates by analyzing fluvial sediment samples collected from source valley alluvial channels draining small, steep, lithologically homogeneous basins in the Iron Mountains ($n=3$), and the Granite Mountains ($n=2$) (Fig. 1). Each of these samples represents the integration of sediment transported out of many small sub-basins and mixed by fluvial processes.

4.1.2. Transect samples of piedmont sediment

Five transects were laid out on the Iron and Granite Mountain piedmonts. The transects were parallel to the range fronts and were spaced at 1-km intervals

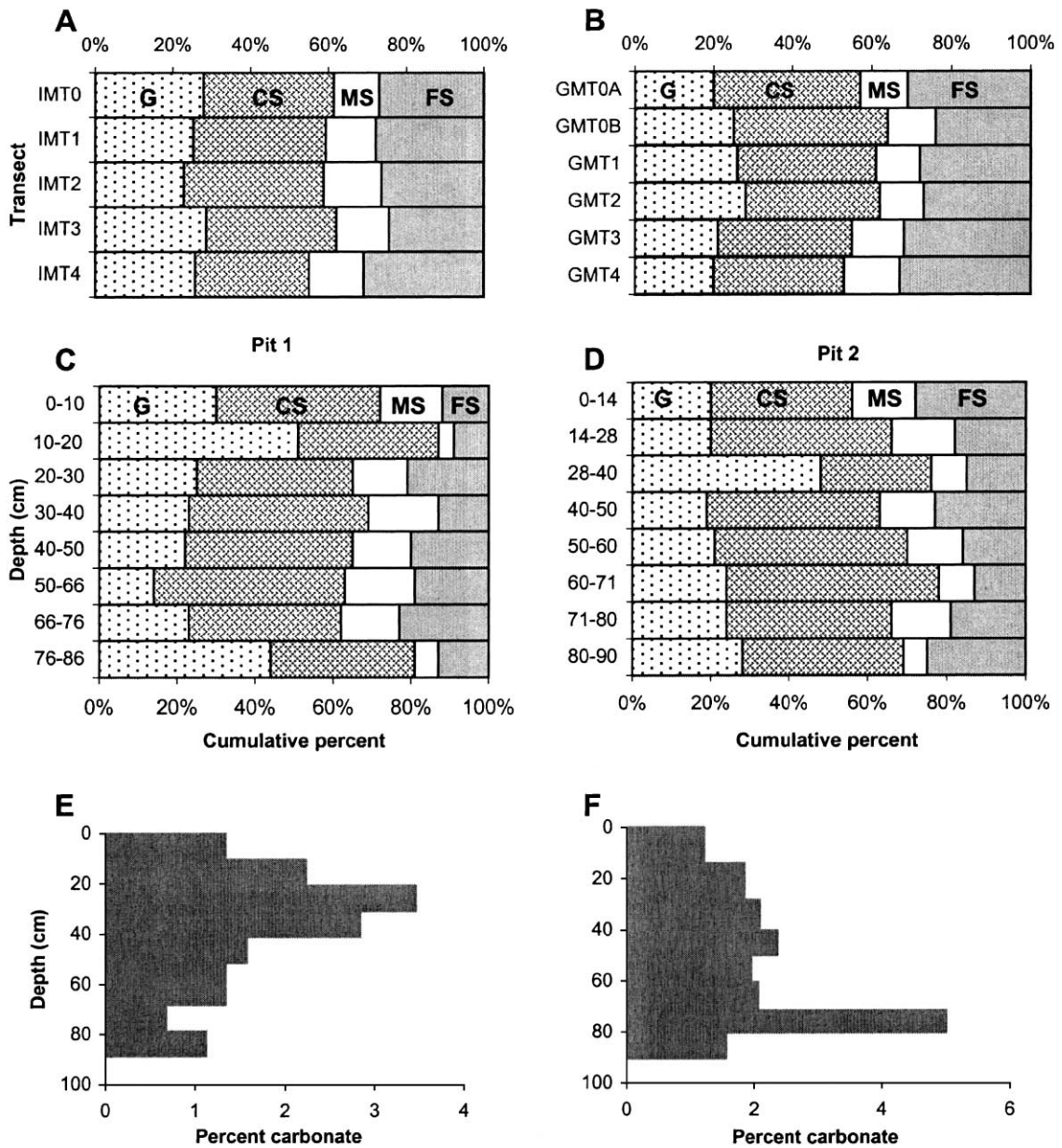


Fig. 2. Grain size and carbonate distribution of sediment collected from Iron and Granite Mountain piedmonts. G=gravel and larger, CS=coarse sand, MS=medium sand, and FS=fine sand and smaller. (A) Amalgamated Iron Mountain transect samples. No clear down-piedmont fining trend is observed. (B) Amalgamated Granite Mountain transect samples. No clear down-piedmont fining trend is observed. (C) Soil Pit 1. Grain size is uniform except for a gravel layers at depths of 10 to 20 cm and 76 to 86 cm. (D) Soil pit 2. Grain size is uniform except for gravel layer at depth of 28 to 40 cm. (E) Soil pit 1 carbonate percentage in less than 80 μ m fraction. Highest percentage is from 20 to 30 cm. (F) Soil pit 2 carbonate percentage. Highest percentage is from 71 to 80 cm.

down the piedmont, starting at the respective range-fronts. Along each transect, we collected equal volumes of surface sediment (0 to 10 cm deep) from 20 sampling stations and amalgamated these 20 samples. The transects were 4 km long and the sampling stations were spaced approximately 200 m apart (Fig. 1). The actual locations of predetermined sampling stations were established in the field using a hand-held Garmin 12 Global Positioning System (GPS); the horizontal uncertainty of uncorrected GPS measurements effectively randomized (± 20 m) actual sample locations along the transects.

The piedmont consists of three distinct, low-relief geomorphic units: low terraces 10 to 20 cm high), active channels, and animal burrow piles (Fig. 3). We classified each transect sampling station according to the geomorphic unit that was sampled (Table 1). To determine if low-terrace sediment has been exposed on average longer than channel sediment and, thus, is more heavily dosed by cosmic radiation, we collected separate subsamples on two transects of both geomorphic units and compared the nuclide activities. We also subsampled sediment from animal burrow piles to determine the depth from which sediment was transported vertically by burrowing. At each of the 20 sampling stations along transects IMT-1 and IMT-

4, we collected equal volumes of sediment from the nearest terrace, channel, and animal burrow pile, and amalgamated each type of sample separately.

A distinctive, rougher fan surface appeared to extend into the northern four sampling stations along IMT-0 (Fig. 1). Channels were entrenched and the surface had a poorly developed pavement. To determine whether or not the difference in appearance was reflected in nuclide activity, we collected a separate subsample of sediment from only the four sampling stations on the alluvial fan surface and amalgamated these samples (IMT-0FAN). The IMT-0 transect sample contained sediment from all 20 sampling stations (Table 1).

4.1.3. Soil pit sediment samples

In the two soil pits on the Iron Mountain piedmont (Fig. 1), we noted soil stratigraphy, sediment grain size, and soil horizonation to a depth of about 1 m. On the basis of soil stratigraphy, we divided each pit into eight depth intervals that we sampled to determine nuclide activity. Each interval was continuous so that the entire soil profile was represented. We dug 25 additional shallow soil pits along IMT-1, IMT-2H, and IMT-4 to understand better the spatial variability of depth to the buried B-horizon.



Fig. 3. Photograph of ephemeral channels and terraces located near IMT-3. Unvegetated channel bottom contains the most recently transported sediment. Low terraces have sparse vegetation. There is no desert pavement. The channel in the middle of photograph is ~ 2 m wide. Photograph taken looking southwest with the Iron Mountains in the right background.

Table 1
Distribution of geomorphic unit sampling stations along transect

Sample ^a	Terrace	Channel bottom	Channel bank	Road	Animal burrow	Alluvial fan	Total of subsamples
IMT-0	11	5	0	0	0	4	20
IMT-0 FAN	0	0	0	0	0	4	4
IMT-1	13	4	1	0	0	2	20
IMT-1 CHAN	0	20	0	0	0	0	20
IMT-1 TERR	20	0	0	0	0	0	20
IMT-1 CRIT	0	0	0	0	20	0	20
IMT-2	13	6	0	1	0	0	20
IMT-3	9	10	0	1	0	0	20
IMT-4	15	5	0	0	0	0	20
IMT-4 CHAN	0	20	0	0	0	0	20
IMT-4 TERR	20	0	0	0	0	0	20
IMT-4 CRIT	0	0	0	0	20	0	20
GMT-0A	13	5	2	0	0	0	20
GMT-0B	10	7	1	1	1	0	20
GMT-1	12	8	0	0	0	0	20
GMT-2	12	8	0	0	0	0	20
GMT-3	11	6	2	1	0	0	20
GMT-4	11	6	2	1	0	0	20

^a GMT=Granite Mountain transect samples, IMT=Iron Mountain transect samples, IMT-0 FAN=sediment from higher alluvial surface, IMT-#CHAN=Iron Mountain channel sediment, IMT-#TERR=Iron Mountain low terrace sediment, IMT-#CRIT=Iron Mountain animal burrow sediment GMT-0A and GMT-0B are field replicates sampled independently.

4.2. Laboratory methods

All samples were sieved and weighed. We analyzed the 0.5 to 1.0 mm size fraction to minimize inclusion of aeolian input from other basins. We did not analyze different grain sizes because ephemeral channels, such as those on the Iron and Granite Mountain piedmonts, are not armored and apparently do not preferentially transport smaller grain sizes (Laronne and Reid, 1993; Laronne et al., 1994; Reid and Laronne, 1995). This conclusion is supported by previous research in arid-region streams that suggests that all grain sizes have statistically similar ¹⁰Be and ²⁶Al activities (Clapp et al., 2000; Clapp et al., 2001). Thus, we assume that nuclide activities in the 0.5 to 1.0 mm size fraction that we analyzed are representative of all fluvially transported material.

We measured the density and carbonate content of all soil pit depth intervals. To measure the density, we extracted a known volume of sediment from each layer and weighed each sample. The density did not vary systematically with depth and the average density of all strata was $1.55 \pm 0.07 \text{ g cm}^{-3}$. We used the Chittick apparatus to measure carbonate content (Machette, 1986). Based on the results of the carbonate measurements (Fig. 2) and our soil pit observa-

tions, we classified the carbonate development as Stage I.

Samples for nuclide analysis (0.5 to 1 mm) were ultrasonically etched, once in heated 6 N HCl and up to four times in heated 1% HF and 1% HNO₃ in order to remove any atmospheric ¹⁰Be and to isolate at least 40 g of pure quartz (Kohl and Nishiizumi, 1992). After the addition of 250 µg of Be carrier, we digested the samples with HF. Be and Al were purified using chromatographic techniques. The ¹⁰Be/⁹Be and ²⁶Al/²⁷Al ratios were determined using accelerator mass spectrometry (AMS) at Lawrence Livermore National Laboratory. All measurements were corrected using similar-sized procedural blanks. Blanks were prepared with each batch of seven samples and analyzed at the same time as the other seven samples. We calculated ¹⁰Be and ²⁶Al activity from ⁹Be (added as carrier) and native ²⁷Al measured by Inductively Coupled Argon Plasma Spectrometry–Optical Emission in duplicate aliquots removed from HF solutions.

4.3. Reproducibility

The nuclide data are reproducible. Field replication, laboratory replication (Table 2), and the ²⁶Al/¹⁰Be

Table 2
 ^{10}Be and ^{26}Al data for the Iron and Granite Mountain piedmonts

Sample ^a	Elevation (m) ^b	Northing ^{c,d}	Easting ^{c,d}	Measured nuclide concentration (10^6 atoms g^{-1}) ^e		Ratio $^{26}\text{Al}/^{10}\text{Be}$	Description
				^{10}Be	^{26}Al		
GMV-1	485	3766547	671919	0.168 ± 0.009	1.02 ± 0.06	6.08 ± 0.48	integrated valley sediment
GMV-2	600	3764501	672404	0.131 ± 0.005	0.82 ± 0.04	6.22 ± 0.40	integrated valley sediment
GMV-3	550	3765000	672274	0.148 ± 0.005	0.98 ± 0.05	6.65 ± 0.41	integrated valley sediment
GMT-0A	450	3767980	670920	0.188 ± 0.009	1.15 ± 0.06	6.10 ± 0.46	integrated transect sediment (20 sites)
GMT-0B		3766620	674540	0.191 ± 0.010	1.06 ± 0.10	5.58 ± 0.59	field replicate of GMT-0A
GMT-1	415	3768900	671270	0.213 ± 0.015	1.11 ± 0.16	5.21 ± 0.86	integrated transect sediment (20 sites)
GMT-2		3767530	674920	0.243 ± 0.010	1.57 ± 0.08	6.46 ± 0.42	integrated transect sediment (20 sites)
GMT-3	350	3769820	671640	0.290 ± 0.011	1.66 ± 0.10	5.71 ± 0.41	integrated transect sediment (20 sites)
GMT-4		3768440	675260	0.316 ± 0.012	1.95 ± 0.10	6.18 ± 0.39	integrated transect sediment (20 sites)
IMV-1	530	3770760	672000	0.140 ± 0.004	0.91 ± 0.06	6.46 ± 0.46	integrated valley sediment
IMV-2		3769400	675620	0.162 ± 0.005	1.13 ± 0.07	6.93 ± 0.47	integrated valley sediment
IMV-3	495	3776603	666643	0.143 ± 0.004	0.99 ± 0.06	6.89 ± 0.45	integrated valley sediment
IMT-0	425	3775699	666478	0.226 ± 0.010	1.38 ± 0.08	6.14 ± 0.45	integrated transect sediment (20 sites)
IMT-0FAN		3777034	668460	0.212 ± 0.008	1.37 ± 0.11	6.46 ± 0.57	integrated alluvial fan sediment (4 sites)
IMT-1	400	3773103	668011	0.245 ± 0.008	1.46 ± 0.07	5.98 ± 0.36	integrated transect sediment (20 sites)
IMT-1CHAN		3777034	668460	0.252 ± 0.011	1.51 ± 0.08	6.00 ± 0.42	integrated channel sediment (20 sites)
IMT-1CRIT		3776442	668402	0.259 ± 0.008	1.68 ± 0.09	6.51 ± 0.40	integrated animal burrow sediment (20 sites)
IMT-1TERR				0.258 ± 0.011	1.53 ± 0.10	5.95 ± 0.46	integrated terrace sediment (20 sites)
IMT-2	355	3776816	670422	0.286 ± 0.009	1.87 ± 0.11	6.54 ± 0.43	integrated transect sediment (20 sites)
IMT-3		3772997	669974	0.320 ± 0.013	2.04 ± 0.12	6.37 ± 0.46	integrated transect sediment (20 sites)
IMT-3DUP	320	3776850	671359	0.325 ± 0.010	1.90 ± 0.10	5.86 ± 0.35	laboratory replicate of IMT-3
IMT-4		3772898	670988	0.367 ± 0.100	2.38 ± 0.12	6.49 ± 0.36	integrated transect sediment (20 sites)
IMT-4CHAN	290	3776693	672391	0.393 ± 0.019	2.16 ± 0.13	5.49 ± 0.42	integrated channel sediment (20 sites)
IMT-4CRIT		3772847	671975	0.392 ± 0.019	2.24 ± 0.12	5.71 ± 0.41	integrated animal burrow sediment (20 sites)

Table 2 (continued)

Sample ^a	Elevation (m) ^b	Northing ^{c,d}	Easting ^{c,d}	Measured nuclide concentration (10 ⁶ atoms g ⁻¹) ^e		Ratio ²⁶ Al/ ¹⁰ Be	Description
				¹⁰ Be	²⁶ Al		
IMT-4TERR				0.380 ± 0.020	2.24 ± 0.12	5.89 ± 0.43	integrated terrace sediment (20 sites)
PIT1 0-10	405	3774990	679030	0.194 ± 0.015	1.10 ± 0.08	5.67 ± 0.57	integrated soil pit sediment
PIT1 10-20				0.193 ± 0.007	1.21 ± 0.08	6.29 ± 0.45	integrated soil pit sediment
PIT1 20-30				0.299 ± 0.014	1.73 ± 0.11	5.80 ± 0.44	integrated soil pit sediment
PIT1 30-40				0.328 ± 0.011	2.01 ± 0.10	6.12 ± 0.38	integrated soil pit sediment
PIT1 40-50				0.352 ± 0.011	2.09 ± 0.11	5.94 ± 0.36	integrated soil pit sediment
PIT1 50-66				0.385 ± 0.013	2.51 ± 0.13	6.52 ± 0.40	integrated soil pit sediment
PIT1 66-76				0.403 ± 0.020	2.44 ± 0.14	6.06 ± 0.45	integrated soil pit sediment
PIT1 76-86				0.427 ± 0.026	2.51 ± 0.13	5.89 ± 0.47	integrated soil pit sediment
PIT2 0-14	310	3774990	671500	0.404 ± 0.012	2.54 ± 0.13	6.29 ± 0.38	integrated soil pit sediment
PIT2 0-14DUP				0.441 ± 0.013	2.38 ± 0.12	5.38 ± 0.32	laboratory replicate of PIT2 0-14
PIT2 14-28				0.411 ± 0.016	2.65 ± 0.15	6.44 ± 0.44	integrated soil pit sediment
PIT2 28-40				0.468 ± 0.015	2.74 ± 0.14	5.86 ± 0.36	integrated soil pit sediment
PIT2 40-50				0.473 ± 0.015	2.99 ± 0.15	6.33 ± 0.38	integrated soil pit sediment
PIT2 50-60				0.479 ± 0.016	2.91 ± 0.16	6.08 ± 0.40	integrated soil pit sediment
PIT2 60-71				0.477 ± 0.014	2.84 ± 0.16	5.95 ± 0.37	integrated soil pit sediment
PIT2 71-80				0.496 ± 0.015	3.00 ± 0.15	6.05 ± 0.34	integrated soil pit sediment
PIT2 80-90				0.513 ± 0.015	3.00 ± 0.15	5.84 ± 0.33	integrated soil pit sediment

^a GMV = Granite Mountain valley samples, GMT = Granite Mountain transect samples, IMV = Iron Mountain valley samples, IMT = Iron Mountain transect samples, IMT-0FAN = sediment from higher alluvial surface, IMT-#CHAN = Iron Mountain channel sediment, IMT-#CRIT = Iron Mountain animal burrow sediment, IMT-#TERR = Iron Mountain low terrace sediment, PIT1 = soil pit 1 sediment, PIT2 = soil pit 2 sediment, DUP = laboratory replicate.

^b Measured from Granite Pass and East of Granite Pass U.S.G.S. quadrangles, 1985, average elevation for transect samples.

^c Measured using Garmin 12 GPS, UTM zone 11S, NAD 27 coordinate system.

^d Transect samples are denoted by the two endpoint coordinates.

^e Error is counting statistics of AMS, with 2% uncertainty for stable Be and 4% uncertainty for stable Al combined quadratically.

regression validate the method of collecting integrated samples and the laboratory procedures. Measured yields of Be carrier average $100.6 \pm 1.1\%$; measured yields of Al blanks average $99.7 \pm 0.9\%$, indicating high recovery of stable Al. Nuclide activities of GMT-

0A and B, collected independently along the same transect, are statistically indistinguishable for both ²⁶Al and ¹⁰Be activity (Fig. 4). IMT-3 was analyzed twice; both analyses produced statistically similar results for both ²⁶Al and ¹⁰Be (Fig. 4). Considering the

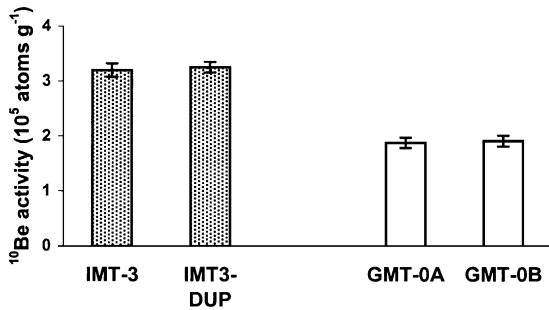


Fig. 4. Reproducibility of sediment samples. GMT-0A and GMT-0B were collected independently. IMT-3 and IMT-3DUP are laboratory replicates. Error bars represent 1σ analytical error.

entire data set, ^{10}Be and ^{26}Al are well correlated with a ratio of 5.8 ± 0.2 and an intercept of $0.07 \pm 0.5 \times 10^5$ atoms at a 68% confidence level (Fig. 5). Since the ^{26}Al data mirror the ^{10}Be data, we focus discussion, for the most part, on the ^{10}Be data. None of our samples have $^{26}\text{Al}/^{10}\text{Be}$ ratios low enough to suggest significant burial on the 10^5 year time scale.

5. Results

Three independent data sets help us understand sediment transport processes and estimate rates of landscape change on the Iron and Granite Mountain piedmonts. Integrated transect nuclide data allow estimation of sediment transport rates down the piedmonts. Soil development, soil pit nuclide data, and ephemeral channel depths in two soil pits reflect the

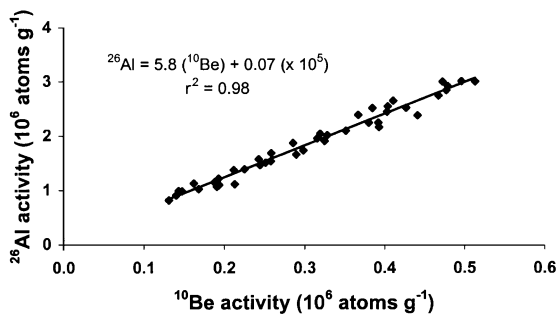


Fig. 5. ^{10}Be and ^{26}Al data are well correlated ($r^2=0.98$). Slope of 5.8 ± 0.2 (68% confidence level) is consistent with production ratio of 6.0 (Nishiizumi et al., 1989) and suggests that sediment samples were not buried for significant periods of time ($>10^5$ years).

depth to which piedmont sediment is well-mixed and, thus, surface histories at these two specific sites. Nuclide activity in source valley alluvial sediment samples allows us to quantify the sediment flux to the piedmonts from mountain drainage basins. Together, these data provide a four-dimensional (including time) view of sediment movement into and across the Iron and Granite Mountain piedmonts on a 10^4 to 10^5 year time scale.

5.1. Piedmont sediment transect data

Integrated transect samples show a remarkably regular increase in nuclide activity down gradient, the rate of which is statistically indistinguishable between the two piedmonts (Fig. 6). The similarity of the transect sample regression slopes suggests that cosmic ray dosing rates, as a function of distance down both piedmonts, are similar. In addition, the nuclide activity (^{10}Be and ^{26}Al) in terrace, channel, and burrow

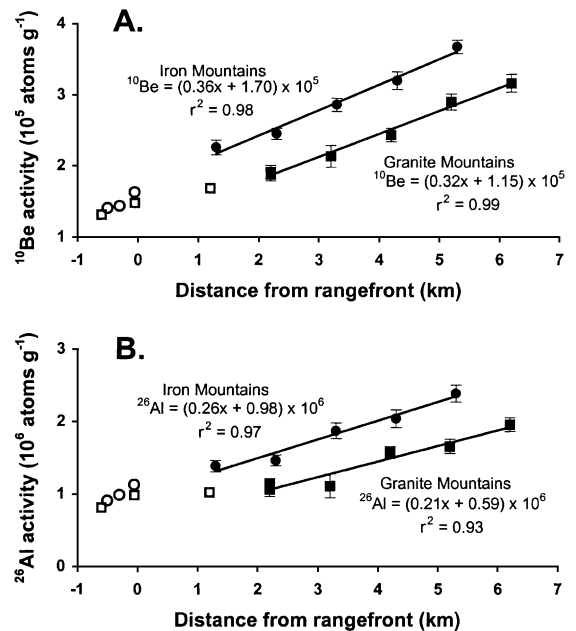


Fig. 6. Transect (closed symbols) and valley (open symbols) data from Iron (circles) and Granite (squares) Mountain piedmonts. (A) ^{10}Be transect data. (B) ^{26}Al transect data. Slopes for nuclide activity as a function of distance from range front are indistinguishable at the 68% confidence level. Error bars represent 1σ analytical error. Error bars for valley samples are same size as symbols.

pile sediment is indistinguishable across gradient (Fig. 7). Similar nuclide activities between channel and terrace sediment imply that channels migrate across the surface on a time-scale comparable to or less than the average cosmogenic nuclide detection limit (the time required to produce the number of atoms that the AMS could count outside the 1σ error, or about 1000 years at our sites). The similarity between nuclide activity in animal burrow sediment and that in terrace and channel sediment suggests that sediment is well mixed to the depth that most animals burrow, presumably less than or equal to the depth of ephemeral channel incision. Sediment on the alluvial fan surface (IMT-0FAN) is no more highly dosed than sediment on the adjacent active piedmont surface (Tables 1 and 2), implying that sediment exposure histories on a 10^3 year time scale are similar along IMT-0, regardless of surface topography.

5.2. Soil pit data

Four lines of evidence suggest that the upper 20 to 30 cm of sediment on the Iron Mountain piedmont, and by inference the Granite Mountain piedmont, are vertically well mixed and distinct from underlying material. (1) The top two samples from both soil pits have statistically indistinguishable ^{10}Be activity (Fig. 8). (2) A sharp contact between overlying gray bedded sediment and underlying red massive sediment (also noted in 25 additional shallow pits along transects IMT-1, IMT-2H, and IMT-4), occurs on average 20 to

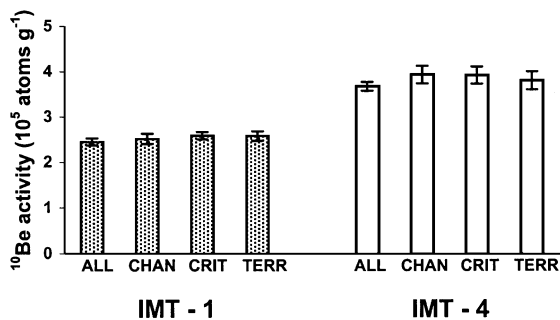


Fig. 7. Different geomorphic units along the same transect have similar nuclide activities. ALL=amalgamated sediment, CHAN=channel sediment, TERR=terrace sediment, and CRIT=animal burrow sediment exposed at surface. Error bars represent 1σ analytical error.

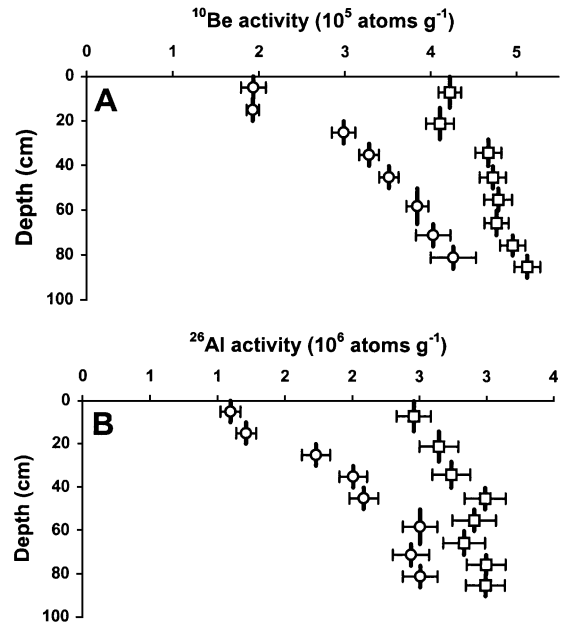


Fig. 8. Data from soil pit samples showing increasing nuclide activities at depth. Pit 1 (circles) is about 2.2 km from the Iron Mountain range front and pit 2 (squares) is about 4.7 km from the Iron Mountain range front. (A) ^{10}Be soil pit data. (B) ^{26}Al soil pit data. Horizontal bars represent 1σ analytical uncertainty. Vertical bars represent thickness of integrated sample.

30 cm below the surface. The underlying reddened material is a buried B-horizon (B_b), the color of which suggests at least several thousand years of stability (Birkeland, 1984). (3) Over 9000 topographic measurements of the ephemeral channels, currently the primary means by which sediment is mixed and transported, show maximum channel depths between 20 and 30 cm, comparable to the depth of bedded sediment overlying the B_b -horizon (Nichols and Bierman, 2002). (4) Transect samples taken from terraces, channels, and animal burrow piles have statistically similar nuclide activities, implying thorough mixing of the uppermost 20 to 30 cm of piedmont sediment on the 10^2 year time scale (Fig. 7).

For the remainder of the paper, we refer to the well-mixed layer, the upper 25 ± 5 cm of piedmont soil as the active transport layer (ATL) (Lekach et al., 1998). We believe that sediment in the ATL is episodically in transport down piedmont because this layer is the same thickness as the maximum channel depths, displays sedimentary structures, and lacks soil develop-

ment. The upper surface of the B_b-horizon defines the base of the ATL.

Soil pit samples are isotopically well mixed in the ATL. However, in the B_b-horizon, nuclide activity increases with depth (Fig. 8). We interpret the distinct discontinuity in nuclide activity between the B_b-horizon and the ATL in soil pit 1 as either: (1) a hiatus in deposition, or (2) erosion of material underlying the current ATL. Consistent with the transect data (Fig. 6), pit 2, located farther from the range front, has higher ¹⁰Be activity than pit 1. Pit 2 has a smaller, and for ²⁶Al, less well-defined step in nuclide activity at the base of the ATL, implying either less erosion or a shorter hiatus in deposition.

5.3. Source valley alluvial sediment data

Average ¹⁰Be activities in source valley alluvial sediment collected along the margins of the Iron and Granite Mountains are $1.49 \pm 0.12 \times 10^5$ (1σ , $n=3$) atoms g⁻¹ and $1.40 \pm 0.05 \times 10^5$ (1σ , $n=2$) atoms g⁻¹, respectively. We did not include GMV-1, because it was not collected at the range front and, thus, its nuclide content does not represent sediment generation rates in the Granite Mountains.

6. Interpretive models of piedmont process

In order to test specific hypotheses and translate our nuclide-based qualitative understanding of piedmont process and process history into quantifiable rates and dates, we used mathematical models to interpret nuclide measurements. One model interprets source valley alluvial sediment samples in terms of drainage basin sediment yield and sediment supply to the piedmont. A second model uses soil pit nuclide depth profiles to infer depositional history (Lal and Arnold, 1985; Phillips et al., 1998). A third model tracks sediment from the time it exits the source basins until it is deposited or is transported past the last transect (Fig. 9).

In order to make our models tractable, we make two simplifying assumptions. First, we assume no preferential dissolution of minerals and, thus, no quartz enrichment in this arid environment (Small et al., 1999). Second, because transit times of sediment across piedmonts are much less than nuclide half lives

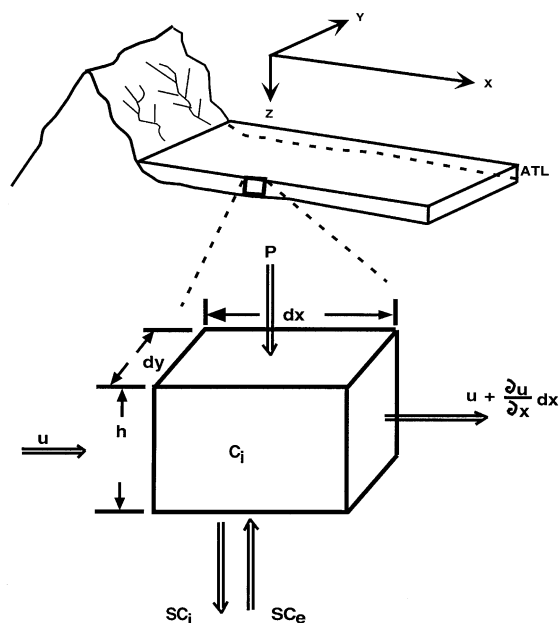


Fig. 9. Schematic of piedmont element model. The piedmont is divided into transport boxes of length, dx , width, dy , and height, h . The double stemmed arrows represent inflows and outflows of nuclides. P is average production during transport, SC_e is erosion from piedmont beneath ATL, SC_i is deposition to the piedmont beneath the ATL, u is the flux from up-gradient, and $u + (\partial u/\partial x)dx$ is the flux out of element box.

and nuclide activity is controlled by surface processes, we disregard radioactive decay.

6.1. Sediment generation model

The long-term average sediment generation rate in the mountain drainage basins that supply sediment to the piedmont is modeled from the cosmogenic nuclide data following the work of Brown et al. (1995), Bierman and Steig (1996), and Granger et al. (1996):

$$m = \frac{AP}{C_i(0)}, \quad (1)$$

where m = long-term average basin-wide lowering rate ($\text{g cm}^{-2} \text{a}^{-1}$), A = neutron attenuation factor (165 g cm^{-2}), P = spatially weighted nuclide production rate ($\text{atoms g}^{-1} \text{a}^{-1}$), and $C_i(0)$ = nuclide activity of sediment leaving the basin (atoms g^{-1}).

Average basin-wide rock lowering rates, based on ¹⁰Be and ²⁶Al production rates in Nishiizumi et al.

(1989) are 37 and 39 m Ma⁻¹, equivalent to sediment fluxes of 0.13 and 0.097 m³ a⁻¹ m⁻¹, from the Iron and Granite Mountains, respectively (Table 3). The basin-wide rock lowering rates, based on production rates in Bierman et al. (1996) are 31 and 33 m Ma⁻¹, equivalent to sediment fluxes of 0.11 and 0.082 m³ a⁻¹ m⁻¹, respectively. The Iron and Granite Mountain denudation rates are comparable to those, estimated from analysis of ¹⁰Be and ²⁶Al in sediment of other landscapes in arid regions. For example, a gneissic sub-basin of Yuma Wash in Arizona is eroding at 30 ± 2 m Ma⁻¹ (Clapp et al., 2002), and the granite, schist, and gneiss of Nahal Yael drainage basin in the Negev Desert are eroding at 29 ± 6 m Ma⁻¹ (Clapp et al., 2000). However, the Iron and Granite Mountains are eroding more slowly than semiarid granitic basins in California (60 ± 14 m Ma⁻¹) and sandstone basins in New Mexico (101 ± 23 m Ma⁻¹) (Granger et al., 1996; Clapp et al., 2001). Erosion rates of granitic landforms are not controlled by precipitation alone as the Iron and Granite Mountains (79 mm a⁻¹ of precipitation) have erosion rates that are similar to those in the much wetter Luquillo Forest in Puerto Rico (~ 43 m Ma⁻¹, >3600 mm a⁻¹ of precipitation) (Brown et al., 1995).

6.2. Soil pit profiles, interpretive model

Soil pit data allow insight into past piedmont processes, specifically the rate at which sediment is added to or lost from the base of the ATL. Stable or eroding surfaces have nuclide profiles that decrease exponentially with depth (Lal and Arnold, 1985) (Fig. 10). In contrast, the nuclide activity in all Iron Mountain soil pit samples collected below the ATL increases with depth (Fig. 8). This increase mandates that the Iron Mountain piedmont must have been a surface of deposition during sometime in the past (Fig. 10).

We can estimate piedmont deposition rates by applying the Lal and Arnold (1985) deposition model to our cosmogenic nuclide soil pit profiles. However, this model assumes constant deposition and does not account for the discontinuity of nuclide activity that we measured at the base of the ATL in both soil pits (Fig. 8). To accommodate the hiatus in deposition that this discontinuity represents, we modify the Lal and Arnold model. Considering the thickness (20 cm at pit 1 and 28 cm at pit 2) and density (1.55 g cm⁻³) of the ATL and its effective shielding of the sediment below, we use an iterative solution to estimate both the deposition rate and the time (represented by the nuclide and physical discontinuity) since deposition ceased

Table 3
¹⁰Be and ²⁶Al erosion rates and associated sediment production rates^a

Valley location	Basin Area (km ²)	Production rate (atoms g ⁻¹ a ⁻¹) ^b		Production rate (atoms g ⁻¹ a ⁻¹) ^b		Erosion rate (m Ma ⁻¹) ^c		Sediment generation rate ^d (10 ⁻² g cm ⁻² a ⁻¹)		Sediment flux (m ³ a ⁻¹ m ⁻¹) ^e	
		²⁶ Al ^f	¹⁰ Be ^g	²⁶ Al ^h	¹⁰ Be ⁱ	²⁶ Al	¹⁰ Be	²⁶ Al	¹⁰ Be	²⁶ Al	¹⁰ Be
Iron Mountain	8.1	55.8	9.4	46.5	7.7	35 (29)	39 (33)	0.91 (0.76)	1.03 (0.86)	0.12 (0.10)	0.14 (0.12)
Granite Mountain	5.7	56.4	9.5	47.0	7.6	38 (32)	40 (34)	1.04 (0.86)	1.08 (0.84)	0.094 (0.079)	0.099 (0.084)

^a Averages for IMV-1,2,3 and GMV-2,3.

^b Basin-wide, weighted average production rate, differences reflect different basin hypsometry.

^c Rock equivalent (2.7 g cm⁻²), erosion rates based on Bierman et al. (1996) in parentheses.

^d Sediment density = 1.55 g cm⁻³, sediment generation rates based on Bierman et al. (1996) in parentheses.

^e Per unit length of range front (m), sediment flux based on Bierman et al. (1996) in parentheses.

^f Based on high latitude sea-level production rate of 36.8 atoms g⁻¹ a⁻¹ (Nishiizumi et al., 1989), scaled to site using Lal (1991), neutrons only.

^g Based on high latitude sea-level production rate of 6.03 atoms g⁻¹ a⁻¹ (Nishiizumi et al., 1989), scaled to site using Lal (1991), neutrons only.

^h Based on high latitude sea-level production rate of 30.4 atoms g⁻¹ a⁻¹ (Bierman et al., 1996), scaled to site using Lal (1991), neutrons only.

ⁱ Based on high latitude sea-level production rate of 5.17 atoms g⁻¹ a⁻¹ (Bierman et al., 1996), scaled to site using Lal (1991), neutrons only.

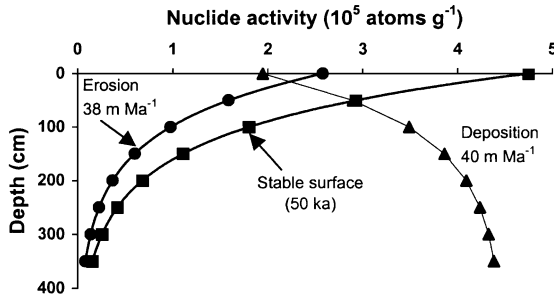


Fig. 10. Stable surfaces (squares) and eroding surfaces (circles) have nuclide activities that decrease at depth. Depositional surfaces (triangles) have nuclide activities that increase with depth. Squares represent a stable surface after 50,000 years of exposure. Circles represent a surface eroding at 38 m Ma^{-1} . Triangles represent a 40 m Ma^{-1} depositional surface. Data are illustrative for Iron Mountain piedmont latitude and elevation and a soil density of 1.55 g cm^{-3} .

(t_h). Implicit in this calculation is the assumption that the ATL existed in its present form and thickness during deposition of the underlying material:

$$N = C_i + \frac{1}{D} \int_0^z P_{\text{ATL}} e^{\left(\frac{-z\rho}{A}\right)} dz + P_o e^{\left(\frac{-h\rho}{A}\right)} t_h$$

$$= C_i + \frac{P_o A}{D\rho} \left[1 - e^{\left(\frac{-z\rho}{A}\right)} \right] + P_o e^{\left(\frac{-h\rho}{A}\right)} t_h, \quad (2)$$

where N =nuclide activity (atoms g^{-1}), C_i =inherited nuclide activity at soil pit location (atoms g^{-1}), D =deposition rate (cm a^{-1}), h =depth of sediment sample in soil pit (cm), P_{ATL} =nuclide production rate at base of ATL ($\text{atoms g}^{-1} \text{ a}^{-1}$), z =depth of sediment sample below the base of the ATL (cm), ρ =soil density (g cm^{-3}), P_o =nuclide production rate at surface ($\text{atoms g}^{-1} \text{ a}^{-1}$), and t_h =time of depositional hiatus (years).

On the Iron Mountain piedmont we have two estimates of C_i . We can use the soil pit data from the ATL to estimate C_i , or we can use the slope of the transect data (Fig. 6) to estimate C_i at the location of each soil pit. We report the average of calculated deposition rates and hiatus lengths for each estimate of C_i . Using the production rate estimates of Nishiizumi et al. (1989), our ^{10}Be and ^{26}Al data suggest long-term steady-state deposition rates of approximately 21 and 45 m Ma^{-1} for pits 1 and 2, respectively (Fig. 11). The average unconformity times for

pits 1 and 2 are 8500 and $10,700$ years, respectively. Using the production rates of Bierman et al. (1996), our ^{10}Be and ^{26}Al data suggest long-term steady-state deposition rates and hiatus times of 17 m Ma^{-1} and $10,300$ years for pit 1 and 37.5 m Ma^{-1} and $12,500$ years for pit 2, respectively (Fig. 11).

These calculations imply a change in piedmont behavior apparently coincident with the Pleistocene/Holocene transition about $10,000$ years ago. Specific-

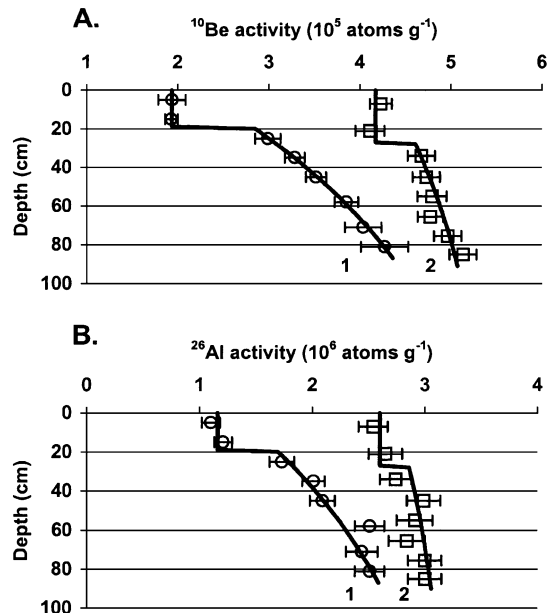


Fig. 11. Predicted deposition rates using (A) ^{10}Be data, and (B) ^{26}Al data for soil pit 1 (circles) and soil pit 2 (squares). Black lines represent model fit. ^{10}Be and ^{26}Al data are consistent and generate similar deposition rates for respective soil pits. Example is based on using Bierman et al. (1996) production rates and soil pit data to estimate C_i . Nuclide data for pit 1 suggest uniform deposition (16 m Ma^{-1}) from the bottom of the soil pit to 20 cm followed by $14,500$ years of stability. Nuclide data for soil pit 2 suggest uniform deposition at 45 m Ma^{-1} from the bottom of the soil pit up to 28 cm followed by 7000 years of stability. A discontinuity in nuclide activities at 20 and 28 cm (Pits 1 and 2, respectively) suggests that an active layer above these depths is transporting but not depositing sediment. Different estimates of C_i , either soil pit data or extrapolation from the slope of transect data (Fig. 6), yield different deposition rates and hiatus times. Using Bierman et al. (1996), nuclide production rates and, averaging the results from the different C_i estimates, yields average deposition rates and hiatus times of 17 m Ma^{-1} and $10,300$ years for pit 1, and 38 m Ma^{-1} and $12,500$ years for pit 2. Using Nishiizumi et al. production rates, the average deposition rate and hiatus time for pit 1 are 21 m Ma^{-1} and 8500 years and for pit 2, 45 m Ma^{-1} and $10,700$ years, respectively.

cally, what had been a transport system in which some mass was lost to the piedmont below, changed to a regime where sediment moved over, and perhaps eroded, previously deposited material. These calculations also imply that sediment was deposited more slowly closer to the range front. Because surface topography on the piedmont is so subdued, these local deposition rates probably represent the depositional histories in a substantial area around each soil pit. Many more pits would be required to map the history of deposition over the entire piedmont.

6.3. Down piedmont sediment transport speeds

In order to quantify the average rate at which grains of sediment move down the Iron and Granite Mountain piedmonts, we used conceptual models that consider both nuclide and mass balances. These models can be developed and employed in a variety of ways (Small et al., 1999; Nichols, 2000). These interpretive models rely upon a variety of parameters some of which we have measured (such as present day ATL thickness and nuclide activity in sediment entering the piedmont), some of which we have calculated (such as mass flux into the piedmont), and some of which we have taken from the literature (nuclide production rates). We do not know how well contemporary measurements of these parameters (such as ATL thickness) represent their value in the past, particularly, in light of changing climate. Therefore, we modeled a variety of different scenarios to test how sensitive sediment transport speeds were to model assumptions and to determine how well our measured data match predictions made using different model assumptions.

The ATL contains a large volume of sediment. The length of the Iron Mountain piedmont is 12–15 km and the average thickness of the ATL is about 25 cm. If the rate at which sediment is currently delivered from the Iron Mountain source area ($0.11 \text{ m}^3 \text{ a}^{-1} \text{ m}^{-1}$) is representative of past rates, then the residence time for the average grain of sediment in the ATL is about 30,000 years. If some of the material in the ATL were derived from erosion of the underlying material, residence time would be shorter. The large volume and long residence time of sediment in the ATL must buffer the system against perturbations in sediment delivery rates, perhaps caused by changing climate.

The simplest model for sediment flux across the piedmont is one in which a column of sediment enters the ATL from the source area and, as successive columns are added at the up-piedmont end, this column moves down the piedmont as a unit. As each column moves down piedmont in this plug flow scenario, it is subjected to cosmic ray bombardment and consequently accumulates ^{10}Be at a rate of about $192 \text{ atoms cm}^{-2} \text{ a}^{-1}$ (Lal, 1988; Bierman et al., 1996 production rates). Here, the cm^2 refers to the surface area of the column, and the column is assumed to be 25 cm high (h), the mean thickness of the ATL. As the measured density of the sediment is 1.55 g cm^{-3} , this amounts to an accumulation rate of $5.0 \text{ }^{10}\text{Be atoms g}^{-1} \text{ a}^{-1}$ in the well-mixed ATL. Sediment moving down the Granite Mountain piedmont acquires ^{10}Be at a rate of about $0.32 \text{ atoms g}^{-1} \text{ cm}^{-1}$ (Fig. 6), implying a speed, u , of $\sim 16 \text{ cm a}^{-1}$ and a flux, uh , of $390 \text{ cm}^3 \text{ cm}^{-1} \text{ a}^{-1}$. This calculated sediment flux is lower by a factor of two than the flux inferred from nuclide activity in the source valley alluvial sediment samples, about $820 \text{ cm}^3 \text{ cm}^{-1} \text{ a}^{-1}$ (Table 3). This model implies that the column would take about 40,000 years to move from the range front to transect GMT4, 6.2 km from the range front.

One can consider other scenarios in order to improve the fit of the model to the data. For example, if erosion of the underlying piedmont is occurring, both sediment and associated nuclides must enter the ATL. Assuming the ATL remains 25 cm thick as indicated by contemporary measurements, the speed of the column must increase with distance from the range front because sediment flux through the ATL is increasing down piedmont. This flux increase will have two offsetting effects. On one hand, the increase in speed will reduce the time available for accumulation of nuclides by production within the column; on the other hand, the more highly dosed sediment eroded from the substrate will increase the average concentration in the column.

Alternatively, we might assume that the ATL is increasing in thickness through time as sediment from the source area is incorporated within it. In this case, with no erosion of the substrate, the speed of the column would decrease down slope. This decrease in speed would lead to a concavity in plots of ^{10}Be activity vs. distance from the range front because, in distal areas, the more slowly moving column would have

more time to accumulate nuclides as it traversed a given distance. Such a concavity is evident in the data for the Granite Mountain piedmont in Fig. 6 although one might argue that it is of marginal statistical significance given the uncertainty in the measurements. There is also a concavity of similar magnitude in the data for the Iron Mountain piedmont if one ignores the measurements between $x = -1$ and $x = 0$. Using the production rate mentioned above and slopes of a smooth concave curve through the Granite Mountain data (Fig. 6), the speed would have to decrease from $\sim 39 \text{ cm a}^{-1}$ in the first kilometer to $\sim 16 \text{ cm a}^{-1}$ between 5 and 6 km from the range front.

To sort out these possibilities, we developed a numerical model of the piedmont. In this model, we divided the ATL into boxes of height, h , length, dx (2000 cm), and width, dy (1 cm) (Fig. 9). The nuclide content of a box increases due to production, P , and erosion of the substrate at a rate S . Thus, during the residence time of sediment in the box, taken to be dx/u , the concentration of nuclides becomes:

$$C_i = C_{i-1} + (P + SC_e) \frac{dx}{uh}. \quad (3)$$

Sediment and nuclides were considered to enter the box from the up-piedmont end. This sediment is then thoroughly mixed with that already in the box and that entering by substrate erosion, thus homogenizing the nuclide concentration. The mixing algorithm is:

$$C_i = \frac{(C_{i-1}u + C_i dx)h + C_u S dx}{(u + dx)h + S dx}, \quad (4)$$

where $C_u = C_e \delta + C_i (1 - \delta)$, and $\delta = 1$ when $S > 0$ and 0 when $S < 0$. The effect of the latter relation is to make the concentration of nuclides in the sediment entering the box through erosion equal to that in the substrate. Finally, sediment is passed out of this box at its distal end and enters the next box downslope.

There are two main differences between the mixing model and the column model described above. The most important is that mixing is allowed between columns and between the underlying piedmont and the ATL. This mimics actual processes on the piedmont where there is exchange between sediment in transport and sediment that has been residing in the ATL for some years. In addition, some lower activity sediment could be deposited from the ATL to the

piedmont below, or some higher activity sediment located in the B_b -horizon below the ATL could be eroded and incorporated into the transport layer. The other key difference is that with a numerical model we can incorporate changes in h , S , and C_e with x .

Using measured parameters, we have generated models that fit the Iron and Granite transect data well (RMS error, 7300 and 10,200 atoms g^{-1} , respectively, Fig. 12). For both these models, we used the nuclide production rates of Bierman et al. (1996), the nuclide-based estimates of sediment flux to the piedmont (Table 3), the soil pit-based estimates of nuclide activity in the top of the underlying B_b -horizon, the

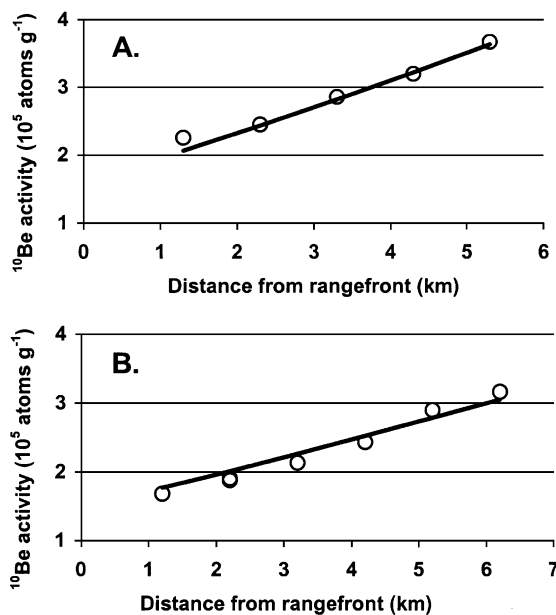


Fig. 12. Predicted (lines) and measured (circles) nuclide activities for Iron (A) and Granite (B) Mountains. Predicted values are from mixing model. RMS errors are low for both Iron Mountain (7.3×10^3 atoms g^{-1}) and Granite Mountain (10.2×10^3 atoms g^{-1}). The following model parameters are the same for both piedmonts: $P_o = 6.3$ atoms $\text{g}^{-1} \text{ a}^{-1}$, $A = 165$ g cm^{-2} , $\rho = 1.55$ g cm^{-3} , $C_e =$ linear extrapolation between nuclide activity in soil pits of upper B_b sample corrected for 5000 years of surface exposure below 25 cm ATL. For Iron Mountain: h_o , the thickness of the ATL at the range front, is 9.0 cm; α , defined as the down piedmont rate of ATL thickening, is 4.4 cm km^{-1} ; h_{dot} , the increase in ATL thickness attributed to incorporation of source valley alluvium sediment, is 0 cm a^{-1} ; q_o , the average basin-wide sediment flux, is 1100 $\text{cm}^3 \text{ a}^{-1} \text{ cm}^{-1}$ (Table 3). For Granite Mountain: $h_o = 16$ cm, $\alpha = 3.2$ cm km^{-1} , $h_{dot} = 0.0003$ cm a^{-1} , $q_o = 820$ $\text{cm}^3 \text{ a}^{-1} \text{ cm}^{-1}$ (Table 3).

average soil density, and the accepted neutron attenuation factor (165 g cm^{-2}). Using the parameters listed above, the only way to fit the measured transect data (Fig. 6) was to vary the thickness of the ATL over time and space.

In order to fit the Iron Mountain data, the ATL thickened down piedmont at a rate of 4.4 cm km^{-1} . This resulted in an ATL that thickened from 9.0 cm at the range front to 32 cm at transect 4. Erosion rates of the underlying piedmont decreased from 27 m Ma^{-1} at the range front to 14 m Ma^{-1} at transect 4. Average grain speed decreased down piedmont from 122 to 65 cm a^{-1} . This model resulted in a total transit time from the range front to transect 4 of 6400 years.

Although measured nuclide activities increased at a similar rate down both piedmonts, model results suggest that the Granite Mountain piedmont behaves somewhat differently than the Iron Mountain piedmont. To fit the Granite Mountain data, we thickened the ATL at a rate of 3.2 cm km^{-1} and allowed deposition of some sediment from the source area into the ATL at a rate of 0.003 cm a^{-1} . The best fit model resulted in an ATL that thickened from 13 cm at the range front to 33 cm at transect 4, 6.2 km away. Erosion rates of the underlying piedmont decreased from 7 to 0.6 m Ma^{-1} over the same distance. Average grain speeds are lower than those on the Iron Mountain piedmont, decreasing down piedmont from 63 to 24 cm a^{-1} . This model resulted in a total transit time from the range front to transect 4 of 17,000 years.

The mixing model results constrain piedmont behavior. Our best fit models for both piedmonts suggest that sediment is being eroded from below and entrained into the ATL, that average grain speed decreases down piedmont, and that the geometry of the ATL changes over time and space. Transit times from the range front to transect 4 range from 6600 to 17,000 years and average grain speed ranges from a few decimeters to a meter per year. Additional soil pit nuclide data and developing models that step through time will probably further increase our understanding of piedmont behavior.

7. What we have learned about desert piedmonts

In situ produced cosmogenic nuclides trace sediment movement onto, across, and within desert

piedmonts. Nuclide data allow us to approach fundamental questions about piedmont behavior that have long resisted quantification such as the rates of sediment transport and deposition across low-gradient desert surfaces. The combination of amalgamated transect samples, source-valley alluvial samples, and soil-pit depth profiles with mass and nuclide balance models represents a new approach to the application of cosmogenic nuclides, one that begins to consider large scale problems in landscape behavior and history through a quantitative understanding of sediment movement and sediment budgets over time and space.

7.1. Piedmonts as dynamic yet organized systems

Nuclide data require that the low gradient granitic piedmonts we studied are dynamic on a variety of length and time scales ranging from years to millennia and meters to kilometers. For example, nuclide analyses and field observations suggest that lateral and shallow vertical sediment mixing processes are important and rapid on granitic desert piedmonts. Mixing is done by animal burrowing and by the random avulsion, incision, and filling of the shallow ephemeral channels that criss-cross the piedmont surface (Nichols and Bierman, 2002). Low-relief (dm-scale) geomorphic units (channels and terraces) have indistinguishable nuclide activities (Fig. 4), suggesting that braided ephemeral channels migrate across the piedmont surface on 10^2 to 10^3 year time scales, reshaping surface microtopography. Depth profiles (Fig. 8) and nuclide analysis of sediment brought to the surface by burrowing animals reveal that the uppermost 20 to 30 cm of piedmont sediment is well and continually mixed over a time scale comparable to that for lateral mixing.

Within this well-mixed system there is order. Nuclide activity increases uniformly down both piedmonts (Fig. 6). The regular increase in average nuclide activity as a function of distance from the range front indicates that the locally and temporally chaotic piedmont sediment transport system functions in a predictable, uniform fashion over length and time scales that our amalgamated samples represent (km) and can resolve (ka). Individual grains are brought down piedmont in an episodic series of transport events, each presumably of varying length, between which the

grains are stored and dosed by cosmic radiation. The regular increase in average nuclide activity down piedmont reflects the slow, episodic, but ongoing transport of grains from mountain sources to the piedmont and ultimately, in the case of some of the finer grains, to playa sinks.

7.2. Piedmont history

Both geologic and isotopic evidence, the marked discontinuity in soil color and nuclide activity at the base of today's well-mixed active layer, require that the behavior and sediment budget of the Iron Mountain piedmont changed during the Late Pleistocene or Early Holocene epoch. Soil pit data (Section 6.2), specifically the general increase in nuclide activity with depth below the ATL, suggest steady deposition occurred on the piedmont prior to about 10,000 years ago at rates between 17 and 45 m Ma⁻¹. In contrast, there is no stratigraphic or isotopic evidence of Holocene deposition from the ATL into the substrate below. As long as there has been rapid channel migration that currently characterizes water and sediment transport on these granitic piedmonts, there will be a well-mixed layer of surface sediment. The thickness of such an ATL through time cannot be constrained by field measurements and likely varies as a result of changes in sediment supply, climate, and piedmont hydrology; however, modeling can suggest reasonable values of ATL thickness in the past.

The end of the Pleistocene was a time when moisture effectiveness and vegetative cover decreased in the Mojave (Spaulding et al., 1983). Bull and Schick (1979) and Bull (1991) argued that such a climate change would result in a pulse of hillslope erosion and, thus, piedmont aggradation as drainage basin soils, no longer well anchored by vegetation and subjected to increasingly variable precipitation, were stripped from hillslopes. Our data are consistent with a piedmont process change at the Pleistocene/Holocene transition that could have been occasioned by a change in sediment yield and basin hydrology. However, even if sediment yield increased as postulated by Bull, soil pit nuclide data clearly show that such an increase did not cause deposition from the ATL to the piedmont below. It is possible that ATL thickness, which is controlled by the depth of migrating ephemeral channels (Nichols and Bierman, 2002), increased

in response to changing runoff patterns and, thus, accommodated sediment stripped from the basins.¹

7.3. Sediment transport rates

Sediment transport rates across desert piedmonts, expressed as average grain speeds, have been unknown until now. Although there remains some uncertainty in nuclide and sediment production rates and in the flux of sediment delivered from the source basins, average grain speeds on the Iron Mountain piedmont range from a few decimeters to a meter per year. Such low speeds imply that human disturbance or sediment contamination would have long-lasting effects on desert piedmonts. Average sediment grains that are not deposited into long-term storage still remain on the piedmont for up to tens of thousands of years as they move from mountains to the playa.

7.4. Application to the "pediment problem"

The piedmonts that we studied are low relief, planar surfaces where sand and fine gravel are transported from the abutting granitic highlands to distant lowland basins. Classifying these piedmont surfaces is not straightforward. They are pediment-like in their planar morphology and in the existence of an active transport layer over an indurated, and perhaps beveled, substrate. They are fan-like in that deposition dominated the piedmont surface over the later Pleistocene.

Whatever term is used to describe the Granite and Iron Mountain piedmonts, our data are consistent with a geomorphic system dominated by rapidly migrating channels, spatially homogeneous braided drainage, planar morphology, and a uniform substrate lithology. Homogeneity of a piedmont drainage network is rep-

¹ One of us (RLH) interprets the available data differently. Although there must be an ATL whenever fluvial deposition is occurring on such a piedmont, Hooke suspects that deposition on this piedmont effectively ceased prior to the last major pluvial period in the Mojave. During this pluvial, runoff may have been confined, by vegetation, to more permanent and more stable channels. During this hiatus, lasting 10 to 20 ka, weathering resulted in the observed red B₀ horizon. Upon return to arid conditions at the end of the Pleistocene, according to this interpretation, channels began to migrate more freely across the piedmont surface and the present ATL began to form from a mixture of new material derived from the source area and old material from erosion of the B₀.

resented numerically by a “random walk” of channels over uniform lithology (Rachocki, 1981). Results of such a model show that where alluvial fans coalesce, drainage becomes an interconnected network of braided channels, the discharge of channels becomes uniform, and the “. . . coalesced surface forms an alluvial piedmont plain.” Individual channel morphometry on the Iron Mountain piedmont does not vary significantly over the piedmont’s width or length (Nichols and Bierman, 2002) consistent with Rachocki’s findings.

Weak channel banks and rapid changes in discharge are typical of migrating channels in sediment-laden networks (Ritter, 1978) and allow for rapid migration of channels over either more resistant bedrock or more indurated sediment. Rapid channel migration, such as we have demonstrated isotopically at Iron Mountain, could effectively bevel high spots on piedmonts and maintain a planar morphology without forming entrenched channels. This lateral erosion process is consistent with the ideas of Gilbert (1877) and Paige (1912), who were the first to speculate that such a process contributes to pedimentation.

7.5. Implications for the application of cosmogenic nuclides to geomorphic problems

This study integrates several different applications of in situ produced cosmogenic nuclides in an attempt to understand better a geomorphic system. The amalgamated transect technique, developed and presented in this paper, averages out point to point differences and elucidates large-scale trends in nuclide activity and, thus, landscape behavior. While sample collection is time intensive, the number of samples generated is modest and the surface area over which the results are relevant is quite large. Simple models allow for determination of a sediment budget for the Iron and Granite Mountain piedmont systems and, thus, calculation of average grain speeds across piedmont surfaces. Depth profiles of nuclide activity in soils allow us to infer past behavior of piedmont systems as well as allowing estimation of sediment deposition rates over time (Lal and Arnold, 1985; Brown et al., 1995; Phillips et al., 1998); however, depth profiles are sample intensive and representative of only modestly sized areas near the soil pit. All of the field and analytical approaches that we have used could be applied in any number of different geomorphic settings.

Measuring and interpreting cosmogenic nuclide activities allow us to quantify sediment transport rates and piedmont processes on a 10^3 to 10^5 year time scale, much shorter than the time of formation of many desert piedmonts (Cooke and Warren, 1973; Oberlander, 1974), but much longer than the duration of contemporary process studies (Abrahams et al., 1984; Lekach and Schick, 1999; Yair, 1999). Thus, our results describe piedmont behavior and piedmont modification and begin to approach the question of piedmont genesis. Such an understanding will only come when a variety of data including underlying structure, lithology, and the geometry of sediment cover are integrated fully with modern process studies, cosmogenic rate data, and mass balance models.

Although this investigation focuses on one area, the similar increase of nuclide activity down both the Iron and Granite Mountain piedmonts suggests that our findings can probably be generalized to other granitic piedmonts in similar tectonic and climatic settings. Applying this technique to piedmonts with different lithologies, slopes, tectonic settings, climates, and morphologies will provide a better understanding of the rate, history, and distribution of desert piedmont processes throughout the world.

Acknowledgements

We thank D. Santos and C. Massey for field assistance, D. Howell for statistical assistance, B. Copans and S. Neis for laboratory assistance, and D. Dethier and S. Brown (Williams College) for assistance with carbonate analyses. E. Steig provided helpful comments on an earlier version of this manuscript. Funding for this project was provided by U.S. Army Research Office grants DAAG559710180 and DAAH049610036, and in part by the U.S. Department of Energy contract No. W-7405-Eng-48, and National Science Foundation grants EAR 9628559 and MRI EAR 9724190.

References

- Abrahams, A.D., Parsons, A.J., Cooke, R.U., Reeves, R.W., 1984. Stone movement on hillslopes in the Mojave Desert, California: a 16-year record. *Earth Surf. Processes and Landforms* 9, 365–370.

- Bierman, P.R., Steig, E.J., 1996. Estimating rates of denudation using cosmogenic isotope abundances in sediment. *Earth Surf. Processes and Landforms* 21, 125–139.
- Bierman, P., Larsen, P., Clapp, E., Clark, D., 1996. Refining estimates of ^{10}Be and ^{26}Al production rates. *Radiocarbon* 38, 149.
- Birkeland, P.W., 1984. *Soils and Geomorphology*. Oxford Univ. Press, New York, 372 pp.
- Brown, E.T., Stallard, R.F., Larsen, M.C., Raisbeck, G.M., Yiou, F., 1995. Denudation rates determined from the accumulation of in situ-produced ^{10}Be in the Luquillo Experimental Forest, Puerto Rico. *Earth Planet. Sci. Lett.* 129, 193–202.
- Bull, W.B., 1977. The alluvial-fan environment. *Prog. Phys. Geogr.* 1, 222–270.
- Bull, W.B., 1991. *Geomorphic Responses to Climatic Change*. Oxford Univ. Press, New York, 326 pp.
- Bull, W.B., Schick, A.P., 1979. Impact of climatic change on an arid watershed: Nahal Yael, southern Israel. *Quat. Res.* 11, 153–171.
- Clapp, E.M., Bierman, P.R., Schick, A.P., Lekach, J., Enzel, Y., Caffee, M., 2000. Sediment yield exceeds sediment production in arid region drainage basins. *Geology* 28, 995–998.
- Clapp, E.M., Bierman, P.R., Nichols, K.K., Pavich, M., Caffee, M., 2001. Rates of sediment supply to arroyos from upland erosion determined using in situ-produced cosmogenic ^{10}Be and ^{26}Al . *Quat. Res.* 55, 235–245.
- Clapp, E.M., Bierman, P.R., Caffee, M., 2002. Using ^{10}Be and ^{26}Al to determine sediment generation rates and identify sediment source areas in an arid region drainage basin. *Geomorphology*.
- Clark, D.H., Bierman, P.R., Larsen, P., 1995. Improving in situ cosmogenic chronometers. *Quat. Res.* 44, 367–377.
- Cooke, R.U., Warren, A., 1973. *Geomorphology in Deserts*. Univ. California Press, Berkeley, 394 pp.
- Denny, C.S., 1967. Fans and pediments. *Am. J. Sci.* 265, 81–105.
- Desilets, D., Zreda, M., 2000. Scaling production rates of terrestrial cosmogenic nuclides for altitude and geomagnetic effects. *Geol. Soc. Am. Abstr. Programs* 31, 400.
- Dohrenwend, J.C., 1987. Basin and range. In: Graf, W.L. (Ed.), *Geomorphic Systems of North America*. Decade of North America Geology. *Geol. Soc. Am., Boulder, Colorado, Centennial Spec.*, vol. 2, pp. 303–342.
- Dunai, T., 2000. Scaling factors for production rates of in situ produced cosmogenic nuclides: a critical reevaluation. *Earth Planet. Sci. Lett.* 176, 157–169.
- Gilbert, G.K., 1877. *Geology of the Henry Mountains (Utah)*. U.S. Geographical and Geological Survey of the Rocky Mountain Region. Washington, DC.
- Granger, D.E., Kirchner, J.W., Finkel, R., 1996. Spatially averaged long-term erosion rates measured from in situ produced cosmogenic nuclides in alluvial sediment. *J. Geol.* 104, 249–257.
- Greenbaum, N., Salmon, O., Gerson, R., Schick, A.P., 1999. Slope runoff in a hyperarid region. In: Lekach, J., Hassan, M.A. (Eds.), *Drainage Basin Dynamics and Morphology: Conference Excursion-Negev Desert (Excursion Guide)*. Hebrew Univ., Jerusalem, pp. 104–110.
- Hooke, R.L., 1968. Steady-state relationships on arid-region alluvial fans in closed basins. *Am. J. Sci.* 266, 609–629.
- Kohl, C.P., Nishiizumi, K., 1992. Chemical isolation of quartz for measurement of in situ-produced cosmogenic nuclides. *Geochim. Cosmochim. Acta* 56, 3583–3587.
- Lal, D., 1988. In situ-produced cosmogenic isotopes in terrestrial rocks. *Ann. Rev. Earth Planet. Sci.* 16, 355–388.
- Lal, D., 1991. Cosmic ray labeling of erosion surfaces: in situ nuclide production rates and erosion models. *Earth Planet. Sci. Lett.* 104, 424–439.
- Lal, D., Arnold, J.R., 1985. Tracing quartz through the environment. *Proc. Indian Acad. Sci.* 94, 1–5.
- Laronne, J.B., Reid, I., 1993. Very high rates of bedload sediment transport by ephemeral desert rivers. *Nature* 366, 148–150.
- Laronne, J.B., Reid, I., Yitshak, Y., Frostick, L.E., 1994. The non-layering of gravel streambeds under ephemeral flood regimes. *J. Hydrol.* 159, 353–363.
- Lekach, J., Schick, A.P., 1999. Sediment transport and sediment yield. In: Lekach, J., Hassan, M.A. (Eds.), *Drainage Basin Dynamics and Morphology: Conference Excursion-Negev Desert (Excursion Guide)*. Hebrew Univ., Jerusalem, pp. 89–97.
- Lekach, J., Amit, R., Grodek, T., Schick, A.P., 1998. Fluvio-pedogenic processes in an ephemeral stream channel. Nahal Yael, Southern Negev, Israel. *Geomorphology* 23, 353–369.
- Machette, M., 1986. Calcium and magnesium carbonates. In: Singer, M.J., Janitzky, P. (Eds.), *Field and Laboratory Procedures Used in a Soil Chronosequence Study*. U.S. Geol. Surv., Reston, VI, pp. 30–33.
- Mayer, L., Bull, W.B., 1981. Impact of Pleistocene–Holocene climatic change on particle size distribution of fan deposits in southwestern Arizona. *Geol. Soc. Am. Abstr. Programs* 13, 95.
- McFadden, L.D., Ritter, J.B., Wells, S.G., 1989. Use of multiparameter relative-age methods for age estimation and correlation of alluvial fansurfaces on a desert piedmont, eastern Mojave Desert, California. *Quat. Res.* 32, 276–290.
- Nichols, K.K., 2000. A multiscale approach to understanding desert piedmonts using cosmogenic isotopes and centimeter-scale surveying. MSc Thesis, Univ. Vermont, Burlington, VT, 264 pp.
- Nichols, K.K., Bierman, P.R., 2002. Fifty-four years of ephemeral channel response to two years of intense military activity during World War II, at Camp Iron Mountain, Mojave Desert, California. In: Ehlen, J., Harmon, R.S. (Eds.), *The Environmental Legacy of Military Operations*. *Geol. Soc. Am. Rev. in Eng. Geol.*, vol. 14, pp. 123–136.
- Nishiizumi, K., Winterer, E.L., Kohl, C.P., Klein, J., Middleton, R., Lal, D., Arnold, J.R., 1989. Cosmic ray production rates of ^{10}Be and ^{26}Al in quartz from glacially polished rocks. *J. Geophys. Res.* 94, 17907–17915.
- NOAA, 1982. Monthly normals of temperature, precipitation, and heating and cooling degree days 1951–1980, California, U.S. National Oceanic and Atmospheric Administration (NOAA), Asheville, NC.
- Oberlander, T.M., 1974. Landscape inheritance and the pediment problem in the Mojave Desert of southern California. *Am. J. Sci.* 274, 849–875.
- Paige, S., 1912. Rock-cut surfaces in desert ranges. *J. Geol.* 20, 442–450.
- Phillips, W.M., McDonald, E.V., Reneau, S.L., Poths, J., 1998. Dating soils and alluvium with cosmogenic ^{21}Ne depth profiles:

- case studies from the Pajarito Plateau, New Mexico, USA. *Earth Planet. Sci. Lett.* 160, 209–223.
- Rachocki, A., 1981. *Alluvial Fans an Attempt at an Empirical Approach*. Wiley, New York, 161 pp.
- Reid, I., Laronne, J.B., 1995. Bed load sediment transport in an ephemeral stream and a comparison with seasonal and perennial counterparts. *Water Resour. Res.* 31, 773–781.
- Ritter, D.F., 1978. *Process Geomorphology*. W.M.C. Brown, Dubuque, IA, 603 pp.
- Small, E.E., Anderson, R.S., Hancock, G.S., 1999. Estimates of the rate of regolith production using ^{10}Be and ^{26}Al from an alpine hillslope. *Geomorphology* 27, 131–150.
- Spaulding, W.G., Graumlich, L.J., 1986. The last pluvial climatic episodes in the deserts of southwestern North America. *Nature* 320, 441–444.
- Spaulding, W.G., Leopold, E.B., van Devender, T.R., 1983. Late Wisconsin paleoecology of the American southwest. In: Wright, H.E. (Ed.), *Late-Quaternary Environments of the United States*—Porter, S.C. (Ed.), *The Late Pleistocene*, vol. 1. Univ. Minnesota Press, Minneapolis, pp. 259–293.
- Wells, S.G., McFadden, L.D., Dohrenwend, J.C., 1987. Influence of Late Quaternary climatic changes on geomorphic and pedogenic processes on a desert piedmont, eastern Mojave Desert, California. *Quat. Res.* 27, 130–146.
- Yair, A., 1999. Sede Boquer research site. In: Lekach, J., Hassan, M.A. (Eds.), *Drainage Basin Dynamics and Morphology: Conference Excursion-Negev Desert (Excursion Guide)*. Hebrew Univ., Jerusalem, pp. 18–51.